ACS APPLIED MATERIALS & INTERFACES

Research Article

www.acsami.org

Multifunctional Superhydrophobic Polymer/Carbon Nanocomposites: Graphene, Carbon Nanotubes, or Carbon Black?

Ashish Asthana,[†] Tanmoy Maitra,[†] Robert Büchel,[‡] Manish K. Tiwari,[†,§] and Dimos Poulikakos*[,†]

[†]Laboratory of Thermodynamics in Emerging Technologies, Department of Mechanical and Process Engineering, [‡]Particle Technology Laboratory, Department of Mechanical and Process Engineering, ETH Zurich, Zurich 8092, Switzerland

Supporting Information

ABSTRACT: Superhydrophobic surfaces resisting water penetration into their texture under dynamic impact conditions and offering simultaneously additional functionalities can find use in a multitude of applications. We present a facile, environmentally benign, and economical fabrication of highly electrically conductive, polymer-based superhydrophobic coatings, with impressive ability to resist dynamic water impalement through droplet impact. To impart electrical conductivity, the coatings were prepared by drop casting suspensions with loadings of different kinds of carbon nanoparticles, namely, carbon black (CB), carbon nanotubes (CNT), graphene nanoplatelets (GNP) and their combinations, in a fluoropolymer dispersion. At 50 wt % either CB or CNT, the nanocomposite coatings resisted impalement by water drops impacting at 3.7 m/s, the highest attainable speed in our setup. However, when tested with 5 vol % isopropyl alcohol−water mixture, i.e., a lower surface tension liquid posing a stiffer challenge with respect to impalement, only the CB coatings retained their impalement resistance behavior. GNP-based surfaces featured very high conductivity ∼1000 S/m, but the lowest resistance to water impalement. The optimal performance was obtained by combining the carbon fillers. Coatings containing CB:GNP:polymer = 1:1:2 showed both excellent impalement resistance (up to 3.5 m/s with 5 vol % IPA−water mixture drops) and electrical conductivity (∼1000 S/m). All coatings exhibited superhydrophobic and oleophilic behavior. To exemplify the additional benefit coming from this property, the CB and the optimal, combined CB/GNP coatings were used to separate mineral oil and water through filtration of their mixture.

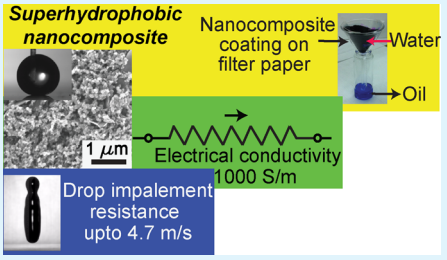

KEYWORDS: *superhydrophobic, multifunctional, nanocomposite, conductive, impalement resistance, oil-water separation*

INTRODUCTION

Superhydrophobic surfaces have established themselves as candidates for various engineering applications, such as self-cleaning, anti-bio-fouling, anti-icing,[1,2] anticorrosion,[3] drag reduction at micro and macro scales[4]and textiles[5] to name a few. Superhydrophobicity provides a pathway toward protecting sensitive properties of the surfaces, which can be easily affected by environmental factors such as rain, dirt, etc. Typically, fabrication of superhydrophobic surface consists of two steps: The first is the controlled generation of an often hierarchical, rough morphology. This is followed by coating this morphology with low energy molecules.[3] In addition to etching, lithography, biomimetic,[6] and stamping processes, superhydrophobic surface morphologies can also be fabricated in a facile manner by dispersing nanoparticles in a matrix of hydrophobic polymer followed by coating the hydrophobic polymer/nanoparticle composite dispersion on any substrate.[7−14]In this case, there is also the potential to take advantage of specific properties of the nanoparticles used to create the rough morphology and generating additional functionalities for the superhydrophobic surface.

The choice of hydrophobic polymer is critical because upon degradation some fluoropolymers are known to form perfluorooctanoic acids (PFOAs), which are developmental toxins dangerous for humans and the environment.[15] In the current work, we employed a commercial fluoroacrylic polymer from DuPont called Capstone ST-100, which does not degrade into PFOAs.[13]

With respect to multifunctional surfaces, one can think of a superhydrophobic surface with additional properties like magnetic,[16] thermal (conductivity),[17] and electrical (conductivity).[7,8,10,11,18,19] These functionalities can be achieved by employing hydrophobic polymers with different properties and/or by using different nanoparticles (zinc oxide,[14] silica,[12]few layers graphene,[20] carbon nanotubes/carbon nanofibers,[8,19] carbon black,[18] etc.).

In the area of multifunctionality, electrically conductive superhydrophobic surfaces are a special case with many attractive applications such as EMI shielding,[21,22] static charge dissipation, electrical circuits,[7] and even regeneration of superhydrophobicity in case of its eventual loss to wetted state.[23] Carbon-based conductive superhydrophobic surfaces are highly important, as they can offer low-cost fabrication along with many exclusive properties that can be offered by carbon allotropes such as extremely high electrical and thermal conductivity of carbon nanotubes (CNT) or graphene, high porosity of carbon black (CB), and impermeability of graphene, among others. There have been several reports of carbon-based

   dx.doi.org/10.1021/am501649w | ACS Appl. Mater. Interfaces XXXX, XXX, XXX−XXX

superhydrophobic surfaces recently. Surfaces based on CNT[24,25] and CB[11,26,27] by themselves were demonstrated to show superhydrophobic behavior without any additional treatment; however, such surfaces showed very poor mechanical durability.[11] Carbon-based nanocomposites on the other hand could overcome many of such difficulties by providing good mechanical properties, while still maintaining high conductivity.[7,10,11,18,19,28]Even though many such surfaces have been developed, very few have shown the ability to retain superhydrophobicity under the impact of a droplet (meniscus impalement resistance).[11,29] Impalement is defined as an event when an impacting droplet does not bounce off from the surface completely and remains attached (as a whole or partially).[2] This nonsticky to sticky behavior directly relates to transition from Cassie−Baxter to Wenzel state.[29] The drop impalement resistance establishes the robustness of the surface and also brings engineered surfaces much closer to the real life applications.

Another important application of superhydrophobic surfaces is oil−water separation.[30] Oil spillage in seawater is a major threat to the environment. It is reported that 258 marine incidents occurred in the period of 1995 to 2005, where dispersants were used to separate oil from water.[31] Use of dispersants remains a matter of disagreement between nations. In this context, a superhydrophobic surface, if it is simultaneously superoleophilic, could be used as an oil/water separator. There are several examples where such surfaces have been used to separate out oil from water.[32,33] A carbon nanoparticle-based superhydrophobic/oleophilic coating (explored in this work) could also be exploited as a filtration membrane for water/oil separator.

Addressing the requirements in the above-mentioned applications requires a simple and versatile approach to superhydrophobicity. We report a facile approach to fabricate highly conductive superhydrophobic nanocomposite coatings consisting of an environmentally benign fluoropolymer matrix with carbon black (CB), carbon nanotubes (CNT), graphene nanoplatelets (GNP), and their combination as nanofillers. Further, environmentally friendly solvents such as acetic acid and water are used in processing. The nanocomposites were characterized for their hydrophobicity, electrical conductivity and meniscus impalement resistance under dynamic conditions. We studied the evolution of these properties with change in particulate loading and in combination of particulates. The resulting superhydrophobic coatings based on CB and CNT demonstrated very high resistance to wetting when subjected to dynamic impact of water droplets. CNT-based surfaces, however, fared poorly with a lower surface tension liquid (5 vol % IPA mixture in water), whereas CB-based surfaces retained their properties with the same liquid. GNP-based surfaces, although the poorest in terms of dynamic impalement resistance, were electrically the most conductive. Coatings employing a combination of CB and GNP possessed the best properties of both the fillers: dynamic meniscus impalement resistance and high electrical conductivity. Also, the oleophilic property of the superhydrophobic nanocomposite coating was utilized by casting the CB and the CB/GNP nanocomposite coating solutions on filter papers which were subsequently used to separate out mineral oil from a mineral oil/water mixture.

EXPERIMENTAL SECTION

Materials. Fluoroacrylic polymer Capstone ST-100 was provided by DuPont Inc. and was used as the fluoropolymer matrix of the coating. It is a 20 weight% dispersion of polymer in water. Acetic acid was purchased from Sigma-Aldrich and used as received. Highly conducting CB powder (ENSACO 250G) was provided by TIMCAL Ltd., Switzerland. CNT (diameter, 110−170 nm; length, 5−9 μm) and GNP with thickness 11−15 nm were procured from Sigma-Aldrich and Ionic Liquid Technologies, Germany, respectively. Solvent Blue 59 (dye content 98%) and Rhodamine B (≥95%, HPLC) were bought from Sigma-Aldrich and used to color the mineral oil and water, respectively, for the oil/water separation experiment. The Whatman qualitative paper, grade 1, diameter 10 cm, was purchased from Sigma-Aldrich.

Methods. Two weight percent fluoropolymer dispersion was obtained by diluting with mixed solvent of acetic acid and deionized water in the ratio of 1:8 by volume. Individual carbon nanoparticles were dispersed in acetic acid with a loading of 2 weight% by an ultrasonic probe (Vibracell VCX 130, 130 W, 20 kHz) for 30 min. Mixtures of CB and GNP were prepared by mixing individual dispersions in various ratios followed by sonication for further 30 min. The fluoropolymer dispersion and the carbon nanoparticle dispersions were mixed to generate the final coating dispersions with different polymer/carbon loadings. The mixture was subjected to sonication for 30 min to achieve homogeneous mixing of fluoropolymer and carbon nanoparticles.

Nanocomposite coatings were prepared by drop casting 150 μL of final dispersions on 25 mm × 25 mm × 1 mm glass substrates. Solvents were evaporated at room temperature in a fume hood. Dried coatings were cured at 160 °C for 30 min in an air oven to melt the polymer[11] and consolidate the coating. The same methodology was followed while preparing the superhydrophobic/oleophilic filter paper, where the nanocomposite coating was cast on Whatman filter paper. Subsequently, the filter paper was used as an oil/water separator.

Characterization. Surface morphology of fabricated superhydrophobic surfaces was evaluated with Field Emission Scanning Electron Microscopy (FESEM Zeiss). For chemical analysis of the surface functional groups Fourier Transfer Infrared (FTIR) spectroscopy (Vector 22, Bruker) was used.

The hydrophobicity of the coatings was characterized by contact angle measurements with water. An in-house level stage, coupled with backlight illumination and CCD camera was used to image drops on substrates. Advancing and receding contact angles were measured by adding or subtracting volume to a drop and imaging when the three phase contact line just starts to move. Images were analyzed with an in-house MATLAB-based image processing code. Minimum three different samples were measured at three random locations for a specific coating composition.

Coating thicknesses were measured with a White Light Interferometer system (Zygo, USA). A step was created in the coatings with a razor blade to measure the thickness. The carbon-based coatings were found to be very absorptive of light and it was needed to deposit a 50 nm layer of gold on top, to be able to carry out the measurements. The gold deposition was performed using electron beam evaporation.

The electrical conductivity of coatings was measured with an impedance analyzer (Solartron SI 1260). A conductive silver paste was used to generate electrodes at a separation of 15 mm on the coated samples. Thin copper wires were connected on these electrodes with a silver paste. A frequency sweep from 1 MHz to 0.1 Hz with 100 mV peak to peak voltage was used to measure the conductivity of coatings. The two point method was used for the measurement.

The drop impalement resistance of coatings was evaluated by investigating the impacts of water droplets released from various heights on the superhydrophobic surfaces. The water drops of diameter ∼2.4 mm were generated using a syringe pump (Harvard Apparatus, Pump 33) feeding a tube with internal diameter of 150 μm. Drops could fall from maximum height of 0.7 m in a test chamber, achieving a maximum impact velocity of 3.7 m/s, limited by the chamber height. Droplet impact events were recorded using a high speed camera (Phantom V9.0) fitted to a macro lens. At least three different locations on each surface and three different samples with the same composition were tested for impalement.

RESULTS AND DISCUSSION

Superhydrophobic surfaces are characterized by a high water contact angle exceeding 150°. Surfaces with exceptionally high contact angles exceeding 170° and very low hysteresis of ~3° have been reported in literature.[34,35] Carbon nanotube-based conductive superhydrophobic surfaces with contact angles ~165° have also been fabricated.[11,36,37] In the current work, we studied how the superhydrophobic performance changes with different carbon fillers (bringing with them additional functionalities) and how it evolves with the particulate loading in the nanocomposite. To this end, our emphasis is on understanding aspects of multifunctional behavior of surfaces and not merely achieving the maximum possible contact angle and minimum possible contact angle hysteresis.

Figure 1 shows a schematic of the surface synthesis employed to form the different nanocomposite coatings. The coatings

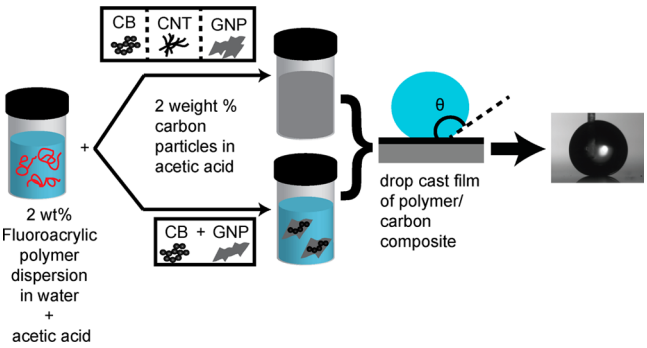

Figure 1. Schematic of the superhydrophobic nanocomposite synthesis using CB, CNT, and GNP nanofillers or their combinations.

with varying carbon nanoparticle/fluoropolymer weight ratio (henceforth designated by ϕ) were cast on a glass substrate. The fluoropolymer used in present study, Capstone ST-100, is a perfluoroalkylethyl acrylate/*n*-alkyl acrylate copolymer with C6 fluoroalkyl chain.[11,38] The exact formula is the manufacturer's proprietary knowledge. However, the knowledge of end functional groups allowed us to interpret the experimental results. For example, acrylic group participates in bonding to surface and contributes to film formation, and perfluoro group imparts it very low surface energy needed for superhydrophobicity.[14] Coatings with five different ϕ values of 0.1, 0.33, 0.5, 1, and 2 were prepared for each of three types of carbon nanoparticles.

Evolution of contact angles and the hysteresis on coatings is shown in Figure 2a–c for CB, CNT, and GNP respectively. At lowest loading of ϕ = 0.1, all the coatings are hydrophobic, but sticky. Thus, the corresponding receding contact angle and hysteresis are not shown for brevity. Contact angle values increased with increasing the loading from ϕ = 0.1 to 0.33 for all three fillers. Both GNP- and CNT-based surfaces are superhydrophobic, displaying advancing contact angle ~160° and hysteresis of 3 and 7°, respectively. The mean advancing contact angle reaches 156° for the CB-based surfaces, but the receding contact angles of the surfaces with ϕ = 0.1 and 0.33 are less than 90°(value not shown in Figure 2). At higher filler loadings (ϕ = 0.5 and greater) both GNP and CNT-based surfaces remain superhydrophobic. CB-based surfaces show excellent superhydrophobicity (both advancing and receding contact angles are as high as 160°) at intermediate values of ϕ (ϕ up to 1), but the receding contact angle turns out to be less than 90° at ϕ = 2, with mean advancing contact angle ~160°.

The mechanical durability of CB (ϕ = 1) based nanocomposite, as a representative surface, was tested using ASTM standard adhesive tape (EN ISO 2409) test. Results are added in a new "Mechanical Durability" section in the Supporting Information. The coating was still superhydrophobic after 6 cycles of tape peel, however, with gradually increasing hysteresis. Clearly, a detailed future work must focus on optimizing the chemical formulation of the host polymer in the nanocomposite in order to enhance the mechanical durability of the coatings, which is beyond the scope of current work that aimed at simultaneous achievement of high electrical conductivity, drop impalement resistance, and the ability to separate oil–water mixtures.

The GNP and CNT surfaces are naturally hydrophobic[39,40] and have been demonstrated to generate superhydrophobic surfaces by simple solvent casting without any further additivies.[20,41] As we will show below, CB has hydrophilic functional groups on its surface as detected by FTIR, which helps explain the loss of superhydrophobicity at high loading of ϕ = 2.

The morphology of the coatings with ϕ = 1 is shown with scanning electron microscopy (SEM) images in Figures 2d, 2e and 2f. Three fillers generate coatings with very distinct morphologies. CB-based coatings (Figure 2d) clearly show the roughness generated by nanoparticles of size ~40 nm. The morphology of CNT-based coatings (Figure 2e) is characterized by a network of entangled nanotubes. The GNP-based surface (Figure 2f) has fish-scale-like texture formed by overlapping GNP sheets.

Water meniscus impalement resistance of the surfaces is of critical importance for the practical application of superhydrophobic surfaces. Impalement dynamics of an evaporating sessile droplet has been previously studied in detail using confocal microscopy and related Laplace pressure rise due to evaporation has been attributed to wetting transition from a Cassie state to Wenzel state.[42] However, a falling drop gives rise to a pressure peak on impact owing to its velocity and this is a crucial event for dynamic impalment.[2] Naturally occurring superhydrophobic surfaces are known to weather pouring rain without loss in superhydrophobicity.[43] In the literature, few surfaces with high meniscus impalement resistance have been developed with laser ablation, micro/nanofabrication techniques etc.[44−48] Brunet et al.[44] observed no impalement for velocity as high as 5.5 m/s on silicon nanowire surfaces. Bird et al.[49] reduced the contact time of impacting droplets with the introduction of special surface morphology. The contact time of droplet decides the energy transfer to a surface and has great significance in anti-icing behavior of superhydrophobic surfaces. We tested the resistance of our coatings against wetting by water droplet impact tests. The Weber number ($We = \rho V^2 d/\gamma$), which signifies relative importance of inertia of droplet to surface tension, is used to characterize the impacts. Here 'ρ' and 'γ' are the density and the surface tension of liquid respectively, 'd' is the droplet diameter and 'V' its velocity. The critical values of velocity and We resulting in droplet impalement on surfaces are designated as V_c and We_c, and are plotted in Figures 2g and 2h, respectively.

GNP-based superhydrophobic surfaces have very low resistance against impalement. The impalement resistance increases with GNP content in the coating. The mean value of V_c remains lower than 0.95 m/s with the corresponding

dx.doi.org/10.1021/am501649w | ACS Appl. Mater. Interfaces XXXX, XXX, XXX–XXX

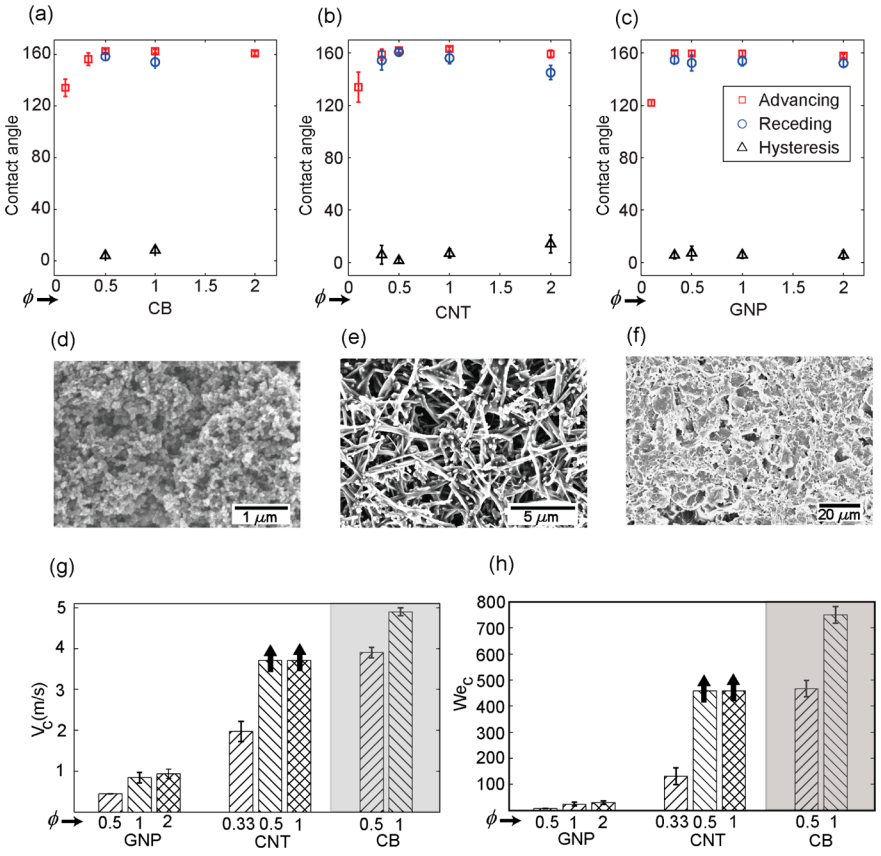

Figure 2. (a–c) Change in contact angle of water with particulate loading in coatings with CB, CNT, and GNP respectively as fillers. SEM images of the coatings with ϕ = 1 for (d) CB, (e) CNT, and (f) GNP. (g) Critical velocity and (h) critical Weber number for drop impalement of the superhydrophobic coatings with change in particulate loading for different fillers. In g and h, the measurements in shaded region were performed using water–IPA mixture drops because of limited experimental chamber height and a scaling law (discussed in text) was used to extract the expected values when using water drops.

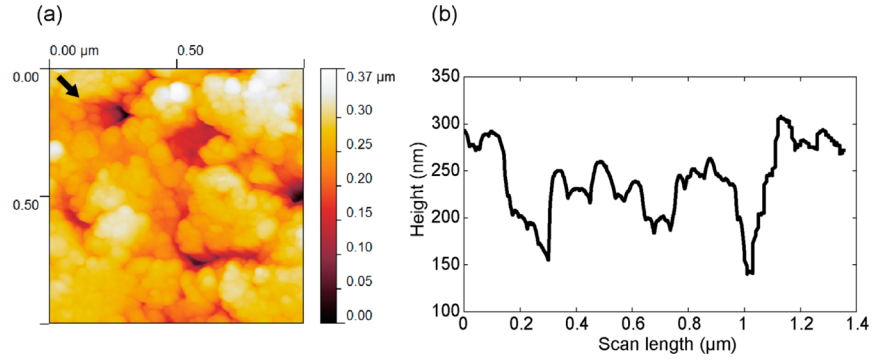

Figure 3. Surface morphology characterization using AFM for CB (ϕ = 1) coating: (a) 1 μm^2 scan, and (b) roughness profile along marked direction in a.

mean We_c being less than 30. The poor water meniscus impalement resistance of GNP/polymer-based superhydrophobic surface can be attributed to the fish-scale morphology of the coating, which results from the flat form of individual GNP flakes having thickness of 11–15 nm and lateral dimension of ~15 μm. CB and CNT-based surfaces perform much better against meniscus impalement. CNT-based coatings with ϕ = 0.33 have V_c of 1.97 ± 0.25 m/s and We_c of 131 ± 33. All other coatings do not show any penetration with the maximum impact velocity of 3.7 m/s attainable in our setup. Thus, to be able to probe the impalement resistance of these surfaces at higher Weber numbers, the liquid surface tension was reduced from 72 to 47.8 mN/m by addition of 5 vol % (vol %) isopropyl alcohol (IPA) to water.[50] The results obtained with IPA–water mixture drops were converted to the equivalent water droplet impact scenario using a scaling law, which suggests that[2] the maximum pressure resulting from a droplet impact is proportional to the capillary pressure, the latter being the maximum pressure originating from the surface tension forces that resist the impalement of the liquid meniscus into the surface texture. The detailed calculations are provided in the Supporting Information.

Using the 5 vol % IPA–water mixture drops, CB-based coatings with ϕ = 0.5 show penetration at 2.9 ± 0.1 m/s which

dx.doi.org/10.1021/am501649w | ACS Appl. Mater. Interfaces XXXX, XXX, XXX–XXX

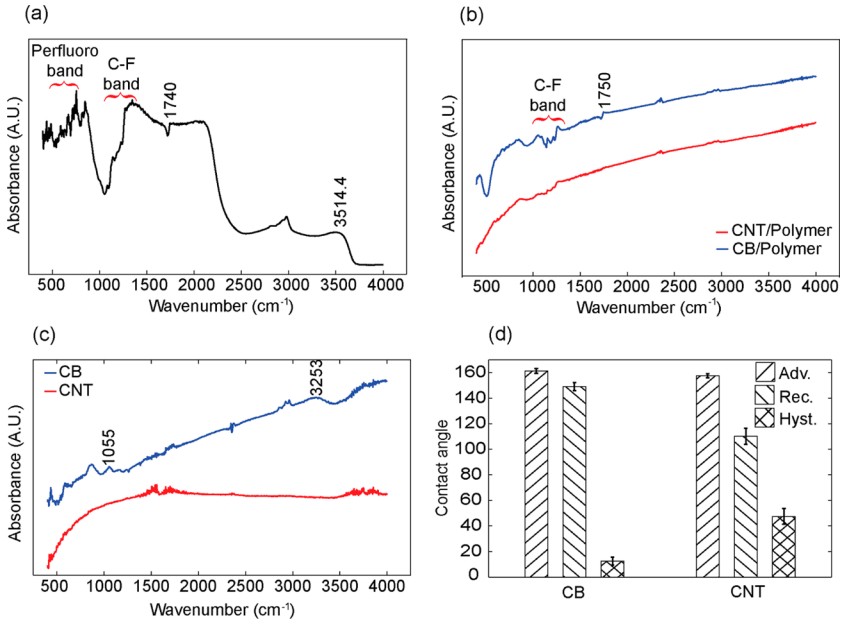

Figure 4. FTIR spectra of (a) a Capstone ST-100 film, (b) a nanocomposite coating with CB and CNT for $\phi = 1$ and (c) the CB and the CNT as received. (d) Contact angle of 5 vol % IPA−water mixture on CB- and CNT-based nanocomposite coating with $\phi = 1$.

increases to 3.66 ± 0.08 m/s for $\phi = 1$. The corresponding mean equivalent, scaled critical velocities for water drops are 3.9 and 4.9 m/s, respectively. The very high critical drop impact velocity of 4.9 m/s for a polymer nanocomposite coating compares well with the highest reported impact resistance up to 5.5 m/s for millimeter size droplets, achieved on a nanowire array.[44]

Atomic Force Microscope (AFM) was used to characterize roughness features of CB ($\phi = 1$) based coating and the result is shown in Figure 3. It was found that these coatings have very low RMS roughness of 46 nm, causing high impalement resistance[2] and very high roughness ratio of 1.93, contributing to good static superhydrophobic parameters, e.g., contact angles.[51] Further, the scan reveals a height variation of 370 nm on a scanned area of 1 μm^2. With RMS roughness being as low as 46 nm, this shows a hierarchical roughness structure on the coating, which explains the low hysteresis of the CB-based coatings.[2] This roughness-based explanation is quite general and can also be used to interpret the low hysteresis measured on the other coatings.

Curiously, the IPA−water mixture drops impacting on CNT-based coatings do not show any rebound even at meager impact height of 5 cm. To ascertain how the nature of these carbon particles is affecting their performance in impalement resistance to lower surface tension liquids like IPA−water mixture (5 vol % IPA), we carried out FTIR spectroscopy on the polymer coatings and on as received CB and CNT powders. The resulting spectra from FTIR are shown in Figure 4.

The FTIR spectrum for the polymer only film in Figure 4a clearly shows a perfluoro-band in 500−750 cm^{-1} and C−F stretching frequency in 1080−1345 cm^{-1}.[52] The sharp peak at 1740 cm^{-1} and the broad peak at 3514 $cm^{-1}$are signatures of C═O and O−H present in −COOH terminal group in fluoropolymer.[9] The spectra of CNT- and CB-based nanocomposite coatings with $\phi = 1$ are shown in Figure 4b. The CB-based coating has a clear C−F band, which is absent at CNT-based coatings indicating a lack of functionalization of CNTs. Moreover, in the CB coating the spectrum contains a shifted C═O peak from 1740 to 1750 cm^{-1} indicating a clear grafting of the polymer to the CB nanoparticles.[9] In order to understand why selectively only CB is functionalized and not the CNTs, the FTIR spectra of dry nanoparticles (both CB and CNTs as received) were obtained without any prior treatment and are shown in Figure 4c. The CNT powder is devoid of any functional groups but CB has a distinct peak at 1055 $cm^{-1}$and a broad peak at 3253 cm^{-1}corresponding to C−O[53] and O−H stretching frequencies. The −OH group on CB can react with the −COOH terminal group in the polymer.[9] This explains the C═O peak shift in the CB-based coating and its absence in the CNT-based coatings.

To illustrate this issue further, Figure 4d shows the contact angle measurements on $\phi = 1$ coatings using 5 vol % IPA−water mixture. Clearly the wetting performance of the CNT-based coating is severely affected by the presence of even such a small amount of IPA in the tested liquid mixture. The advancing contact angle remains the same as in case of pure water, however, the receding contact angle is reduced significantly. In the case of the CB-based nanocomposite coating, the mean hysteresis changes marginally from 8.3 to 12.4°. For the CNT nanocomposite on the other hand, the change is drastic, from 6.9 to 47.5°. This could be attributed to solvophilic graphitic surface of CNT, which does not cross-link with the polymer. A low receding contact angle has been shown to adversely affect the droplet rebound performance of surface.[54] This explains the poor drop impalement resistance of the CNT nanocomposite coating using IPA water mixture as described above.

The electrical conductivity of all the coatings was measured next. The coating thickness was found to be ∼5 μm for all the coatings. This thickness is used to calculate the conductivity values. The results are plotted in Figure 5. For all the tested coatings, the conductivity increases monotonically with carbon filler loading, leveling off at $\phi = 1$. Even at the smallest filler loading of $\phi = 0.1$, the coatings have a mean conductivity of 0.6, 2, and 2.9 S/m for CB, CNT and GNP fillers, respectively. The highest mean conductivity of 950 S/m is achieved for GNP-

dx.doi.org/10.1021/am501649w | ACS Appl. Mater. Interfaces XXXX, XXX, XXX−XXX

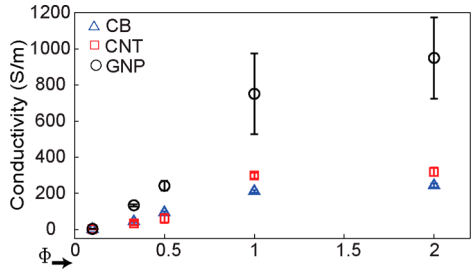

Figure 5. Increase in electrical conductivity of coating with filler loading.

based coatings (at ϕ = 2), which is ~3 times that attained by CNT-based coating with the same filler loading. The CB and CNT-based coatings have similar conductivity for all loadings, with the GNP-based coatings achieving highest values. The higher standard deviation for the GNP-based coatings is a result of inherent inhomogeneity of the GNP/polymer dispersion at higher loadings, which leads to clustering of GNP.

The CB used in the current experiments has particularly high electrical conductivity (with a minimum of 10 S/m with 25% loading in HDPE as per supplier specifications). Metallic multiwalled-CNTs are favored as 1D nanofillers in nanocomposites[55] due to their excellent inherent electrical conductivity in pristine form;[56] however, sample impurities, limited contact between tubes and inevitable tube defects can result in lower conductivity composites.[55] GNP on the other hand have a 2-D structure with 11−15 nm thickness and large lateral dimension (~15 μm). This results in better overlap between contacting particles and very high electrical conductivity for composites.

As is evident from the experiments, CB in coatings imparts the best meniscus impalement resistance and the GNP filler yields the best electrical conductivity. The CNT filler does not offer any particular advantage over the other fillers. This gave impetus to a further study of a mixture of CB and GNP fillers, aiming at obtaining superior all around properties. Note that the combination of carbon nanoparticles has been previously shown to have a synergetic effect on electrical conductivity.[57]

The combined carbon filler loading was fixed at ϕ = 1, because at this value the best impalement resistance for only CB and very high electrical conductivity for only GNP coatings, respectively, was demonstrated. Three CB/GNP weight ratios are tested: 1/3, 1, and 3. All the coatings show advancing contact angle ~160° and mean hysteresis below 5.5°, as shown in Figure 6a. The electrical conductivities of all coatings are plotted in Figure 6b. Both CB/GNP = 1/3 and 1 coatings have very high electrical conductivity at ~1000 S/m, with the coating CB/GNP = 3, being the least conductive at ~640 S/m. Note that the ϕ = 1 coating loaded with GNP alone exhibited a mean conductivity at ~750 S/m (refer to Figure 5) and the corresponding conductivity for the CB only coating was ~200S/m (refer to Figure 5). Therefore, the very beneficial

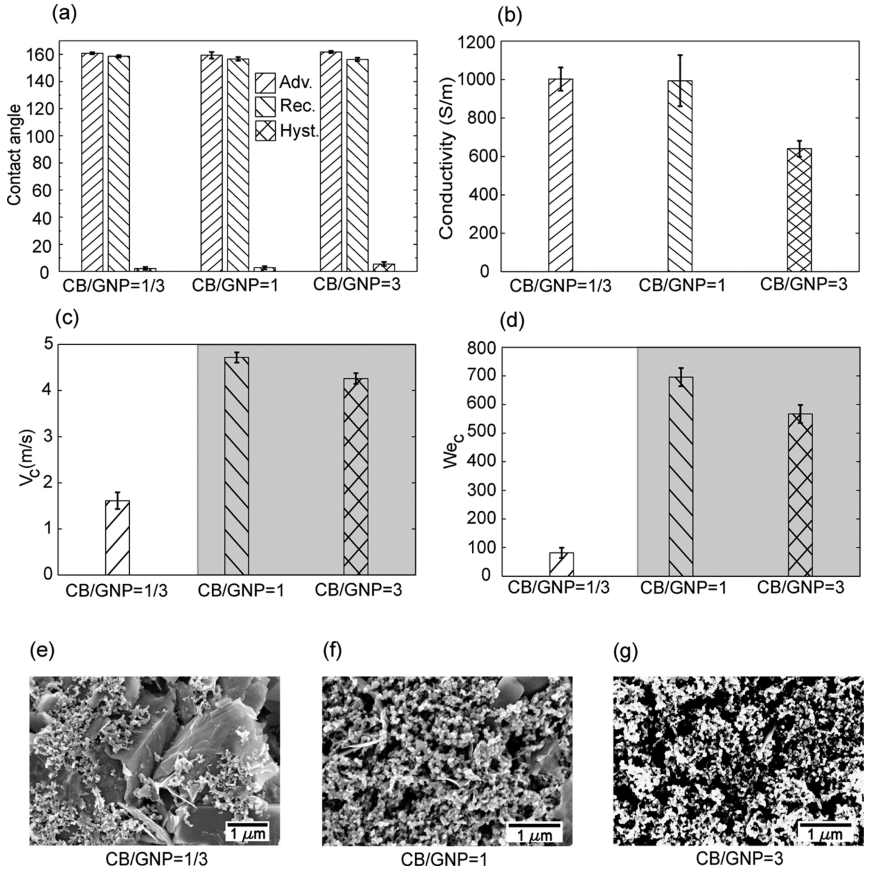

Figure 6. (a) Water drop contact angle, (b) electrical conductivity, (c) critical impalement velocity, and (d) critical Weber number for coatings containing both CB and GNP in varying weight ratio with fixed total filler loading of ϕ = 1. In c and d, the measurements in the shaded region were performed using water-IPA mixture drops, due to the limited experimental chamber height. A scaling law (discussed in text) was used to extract the expected values for water drops (e−g) SEM images of the coatings illustrate the change in morphology with varying weight ratios of CB and GNP.

dx.doi.org/10.1021/am501649w | ACS Appl. Mater. Interfaces XXXX, XXX, XXX−XXX

synergistic effect resulting from mixing CB and GNP is very clear at CB/GNP = 1/3 and 1. The latter is advantageous because GNP is more expensive than CB.

Droplet impact tests also reveal that the addition of CB improves the impalement resistance of coatings, which is very poor with GNP alone. Results of droplet impact tests are shown in terms of V_c and We_c in panels c and d in Figure 6, respectively. Coatings with CB/GNP=1/3 have a mean V_c = 1.60 m/s and a corresponding $We_c \approx 82$, much higher than with GNP alone (refer to Figure 2). Both the CB/GNP = 1 and CB/GNP = 3 surfaces still resist water impalement at the maximum achievable impact velocity of 3.70 m/s. Impact with 5 vol % IPA in water results in impalement at V_c of 3.52 and 3.18 m/s for CB/GNP = 1 and CB/GNP = 3, respectively. Using scaling analysis (see the Supporting Information), this would convert to 4.70 and 4.26 m/s in the case of pure water, for CB/GNP = 1 and CB/GNP = 3, respectively. It is interesting to note that even half the loading of CB in a heterogeneous composite compared to ϕ = 1 coating with CB alone, is sufficient to impart almost identical impalement resistance. Therefore, the demonstrated enhancement and coexistence of both electrical conductivity and impalement resistance make a very strong case for using mixture fillers.

SEM images of these heterogeneous coatings containing two fillers are shown in Figures 6e−g for CB/GNP = 1/3, 1 and 3, respectively. The GNP faces are only sparingly covered with CB for CB/GNP = 1/3, however, both the CB/GNP = 1 and 3 nanocomposites have GNP faces effectively covered with CB. The coverage of GNP with CB results in improved performance against impalement. In addition, CB is known to improve dispersion of GNP by covering up exposed GNP faces and limiting strong van der Waals interaction.[57] The CB incorporated into heterogeneous coating also helps in forming improved conductive pathways between separated GNP sheets. CB covered GNP faces and better dispersion in heterogeneous coatings are possible reasons for the observed improved drop impalement resistance and conductivity. The improvement in dispersion quality and composite properties is not a monotonic function of CB/GNP ratio and could explain the better performance of CB/GNP = 1 compared to CB/GNP = 3. This observation is similar to the behavior of epoxy-based nanocomposites[57,58] with mixture fillers.

All the above-mentioned coatings were found to be oleophilic when tested against mineral oil, with complete spreading of oil drops on coatings. The contact angle of mineral oil on a smooth drop-cast and cured polymer film is measured to be 64°, which is consistent with previously reported contact angle measurements of low surface tension liquids on fluorinated acrylic copolymer surfaces.[59] Rough surfaces with inherently oleophilic chemistry, however, can be made superoleophobic by proper texturing.[60] Re-entrant rough features with overhangs are thought to impart metastable superoleophobicity to such surfaces.[60,61] Certain coating methods such as spray coating have indeed been used for creating superoleophobic polymer nanocomposite coatings.[14,59] Fast solvent evaporation during spraying can cause dry coating with hierarchical features, which lead to superoleophobic behavior.[14] The drop casting method used in present work, however, by the nature of the processing, leaves well settled assembly of nanoparticles, which lacks re-entrant features and consequently lacks oleophobicity. Additionally, the CB surface has domains with graphitic planes and defect or amorphous sites.[62] The defects and amorphous sites contain various functional groups, of which −OH and −COOH take part in binding with the fluoropolymer. Hierarchical morphology as revealed by the AFM scan in Figure 3 also amplifies the role of surface chemistry and enhances wetting with oil. This property of simultaneous existence of superhydrophobicity and oleophilicity is an additional important functionality, which can be used to generate membranes for oil/water separation.

Currently, there exist two competing strategies for oil−water separation, namely: hydrophilic-oleophobic and hydrophobic-oleophilic surface functionalities. Hydrophilic-oleophobic coatings, used for oil−water separation, generally contain polymers with a hydrophobic and a hydrophilic chain. The exact behavior of such surfaces depends on the reorientation of polymer molecule, when in contact with water. The hydrophilic chain, which normally remains buried in bulk to lower the surface energy, becomes reoriented in contact with water to minimize water−polymer interfacial tension. This reorientation of polymer tends to be slow. High separation efficiency has however been achieved with such coatings.[63] Only very recently, instantaneous separation has been reported on such coatings, but with slightly lower efficiency.[64] Such coatings would be useful for gravity driven separation of oil−water mixture as generally oils tend to be lighter than water. On the other hand, coatings with hydrophobic-oleophilic combination (i.e., the category in which surfaces reported in our work belongs to) have been shown to be suitable for high throughput.[65] This combination could be specifically useful in filtration of water in oil emulsions[65] and removing organic contaminants heavier than water, where hydrophilic-oleophobic coatings would be less effective. Apart from that, these coatings could be useful in cases where oil is a small fraction (pollutant) in water. Foams with such functionality have been effectively used to skim oil from the water surface.[66] Moreover, a buried hydrophilic group can ensure better adhesion.

The best performing CB-based nanocomposite at ϕ = 1 and the best heterogeneous nanocomposite with CB/GNP = 1 and ϕ = 1 were coated on Whatman filter papers to form separation membranes. The polymer/CNT-based composites also possess the simultaneous qualities of superhydrophobicity and oleophilicity. Hence, these could also be used for filtration. However, in keeping with our motivation to develop multifunctional superhydrophobic surfaces, only the best performing composites with reference to electrical conductivity and droplet impact were tested for their performance in separation. Figure 7 shows sequences of the oil/water separation test, conducted on

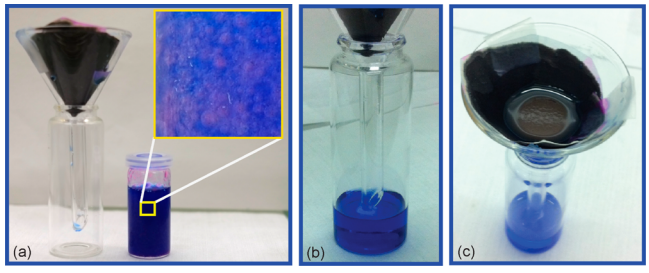

Figure 7. (a−c) Different stages of the oil/water separation experiment. (a) Left-hand side shows superhydrophobic filter paper based on our nanocomposite coating and on the right, a mixture of mineral oil (colored with solvent dye, blue)/water (colored with Rhodamine B, red). Inset shows zoomed view for oil−water emulsion. (b) Separated mineral oil at the bottom of the bottle and (c) separated water remaining in the filter.

dx.doi.org/10.1021/am501649w | ACS Appl. Mater. Interfaces XXXX, XXX, XXX−XXX

a CB/GNP-based membrane. Mineral oil colored with Solvent Blue 59 and water colored with Rhodamine B were used for better visualization. Complete separation was demonstrated. It is noteworthy that while the CB nanocomposite effectively performed the separation of 5 mL of mineral oil mixed with 5 mL of water in ∼15 min, it took ∼24 h to perform the same task with the CB/GNP nanocomposite. This can be attributed to the high barrier efficiency of GNP.[67] A judicious choice of the aforementioned nanocomposites should be exercised, according to the application at hand. The CB/GNP-based nanocomposite, while being optimum for a combination of droplet impact resistance and electrical conductivity, is clearly inferior to the CB-based coating for oil−water separation, when speed of separation is an issue.

CONCLUSIONS

Highly conductive superhydrophobic coatings with high dynamic meniscus impalement resistance were fabricated with a simple, environmentally friendly and economical method using fluoropolymer dispersions of three common kinds of carbon nanoparticles and their combinations. The CB-based coatings were found to be best against impalement resistance, achieving very high critical $We \approx 750$ with 5 vol % IPA−water mixture. GNP-based coatings, even though relatively poor against impalement, featured the best electrical conductivity ∼1000 S/m. A synergistic effect was demonstrated bringing together these excellent individual functionalities into a single composite by combining CB and GNP together as fillers. The CB and the CB/GNP nanocomposites, were coated on filter papers and demonstrated superhydrophobic/oleophilic characteristics, thereby forming simple, well-functioning oil/water separators. By exploiting the facile approach introduced here, these high electrical conductivity superhydrophobic coatings can be easily scaled up and may find use in various applications, for example, in EMI shielding, drag reduction for underwater applications, oil filtration, and enhanced condensation heat transfer.

ASSOCIATED CONTENT

Supporting Information

Details on electrical conductivity calculations and droplet impact scaling analysis. This material is available free of charge via the Internet at http://pubs.acs.org/.

AUTHOR INFORMATION

Corresponding Author

*E-mail: dpoulikakos@ethz.ch. Phone: +41 44 632 27 38. Fax: +41 44 632 11 76.

Present Address

[§]M.K.T. is currently at Mechanical Engineering, University College of London, Torrington Place, London, WC1E 7JE.

Notes

The authors declare no competing financial interest.

ACKNOWLEDGMENTS

The partial support for this work from Swiss National Science Foundation (SNF) grant 200021_135479 is gratefully acknowledged.

REFERENCES

(1) Jung, S.; Tiwari, M. K.; Doan, N. V.; Poulikakos, D. *Nat. Commun.* **2012**, *3*, 615.
(2) Maitra, T.; Tiwari, M. K.; Antonini, C.; Schoch, P.; Jung, S.; Eberle, P.; Poulikakos, D. *Nano Lett.* **2014**, *14*, 172−182.
(3) Xue, C.-H.; Jia, S.-T.; Zhang, J.; Ma, J.-Z. *Sci. Technol. Adv. Mater.* **2010**, *11*, 033002.
(4) Rothstein, J. P. *Annu. Rev. Fluid Mech.* **2010**, *42*, 89−109.
(5) Hoefnagels, H. F.; Wu, D.; de With, G.; Ming, W. *Langmuir* **2007**, *23*, 13158−13163.
(6) Sharma, C. S.; Abhishek, K.; Katepalli, H.; Sharma, A. *Ind. Eng. Chem. Res.* **2011**, *50*, 13012−13020.
(7) Das, A.; Schutzius, T. M.; Bayer, I. S.; Megaridis, C. M. *Carbon* **2012**, *50*, 1346−1354.
(8) Hsu, C.-P.; Chang, L.-Y.; Chiu, C.-W.; Lee, P. T. C.; Lin, J.-J. *ACS Appl. Mater. Interfaces* **2013**, *5*, 538−545.
(9) Hsiang, H.-I.; Liang, M.-T.; Huang, H.-C.; Yen, F.-S. *Mater. Res. Bull.* **2007**, *42*, 420−427.
(10) Bayer, I. S.; Caramia, V.; Fragouli, D.; Spano, F.; Cingolani, R.; Athanassiou, A. *J. Mater. Chem.* **2012**, *22*, 2057−2062.
(11) Bayer, I. S.; Steele, A.; Loth, E. *Chem. Eng. J.* **2013**, *221*, 522−530.
(12) Lakshmi, R. V.; Bharathidasan, T.; Bera, P.; Basu, B. J. *Surf. Coat. Technol.* **2012**, *206*, 3888−3894.
(13) Schutzius, T. M.; Bayer, I. S.; Tiwari, M. K.; Megaridis, C. M. *Ind. Eng. Chem. Res.* **2011**, *50*, 11117−11123.
(14) Steele, A.; Bayer, I.; Loth, E. *Nano Lett.* **2009**, *9*, 501−505.
(15) Lau, C.; Butenhoff, J. L.; Rogers, J. M. *Toxicol. Appl. Pharmacol.* **2004**, *198*, 231−241.
(16) Yoon, M.; Kim, Y.; Cho, J. *ACS Nano* **2011**, *5*, 5417−5426.
(17) Cao, B.-Y.; Kong, J.; Xu, Y.; Yung, K.-L.; Cai, A. *Heat Transfer Eng.* **2013**, *34*, 131−139.
(18) Shen, L.; Ding, H.; Wang, W.; Guo, Q. *Appl. Surf. Sci.* **2013**, *268*, 297−301.
(19) Zhu, Y.; Zhang, J. C.; Zhai, J.; Zheng, Y. M.; Feng, L.; Jiang, L. *ChemPhysChem* **2006**, *7*, 336−341.
(20) Rafiee, J.; Rafiee, M. a; Yu, Z.-Z.; Koratkar, N. *Adv. Mater.* **2010**, *22*, 2151−2154.
(21) Das, A.; Hayvaci, H. T.; Tiwari, M. K.; Bayer, I. S.; Erricolo, D.; Megaridis, C. M. *J. Colloid Interface Sci.* **2011**, *353*, 311−315.
(22) Das, A.; Megaridis, C. M.; Liu, L.; Wang, T.; Biswas, A. *Appl. Phys. Lett.* **2011**, *98*, 174101.
(23) Lee, C.; Kim, C.-J. *Phys. Rev. Lett.* **2011**, *106*, 014502.
(24) Sethi, S.; Dhinojwala, A. *Langmuir* **2009**, *25*, 4311−4313.
(25) Han, Z. J.; Tay, B. K.; Shakerzadeh, M.; Ostrikov, K. *Appl. Phys. Lett.* **2009**, *94*, 223106.
(26) Naha, S.; Sen, S.; Puri, I. K. *Carbon* **2007**, *45*, 1702−1706.
(27) Shen, L.; Ding, H.; Cao, Q.; Jia, W.; Wang, W.; Guo, Q. *Carbon* **2012**, *50*, 4284−4290.
(28) Sansotera, M.; Navarrini, W.; Resnati, G.; Metrangolo, P.; Famulari, A.; Bianchi, C. L.; Guarda, P. A. *Carbon* **2010**, *48*, 4382−4390.
(29) Gu, C.; Ren, H.; Tu, J.; Zhang, T.-Y. *Langmuir* **2009**, *25*, 12299−12307.
(30) Xue, Z.; Cao, Y.; Liu, N.; Feng, L.; Jiang, L. *J. Mater. Chem. A* **2014**, *2*, 2445−2460.
(31) Chapman, H.; Purnell, K.; Law, R. J.; Kirby, M. F. *Mar. Pollut. Bull.* **2007**, *54*, 827−38.
(32) Wang, C.; Yao, T.; Wu, J.; Ma, C.; Fan, Z.; Wang, Z.; Cheng, Y.; Lin, Q.; Yang, B. *ACS Appl. Mater. Interfaces* **2009**, *1*, 2613−2617.
(33) Zhou, X.; Zhang, Z.; Xu, X.; Guo, F.; Zhu, X.; Men, X.; Ge, B. *ACS Appl. Mater. Interfaces* **2013**, *5*, 7208−7214.
(34) Pechook, S.; Kornblum, N.; Pokroy, B. *Adv. Funct. Mater.* **2013**, *23*, 4572−4576.
(35) Sarshar, M. A.; Swarctz, C.; Hunter, S.; Simpson, J.; Choi, C.-H. *Colloid Polym. Sci.* **2012**, *291*, 427−435.
(36) Srinivasan, S.; Praveen, V. K.; Philip, R.; Ajayaghosh, A. *Angew. Chem., Int. Ed. Engl.* **2008**, *47*, 5750−5754.
(37) Luo, C.; Zuo, X.; Wang, L.; Wang, E.; Song, S.; Wang, J.; Wang, J.; Fan, C.; Cao, Y. *Nano Lett.* **2008**, *8*, 4454−8.
(38) Bayer, I. S.; Biswas, A.; Ellialtioglu, G. *Polym. Compos* **2011**, *32*, 576−585.

(39) Werder, T.; Walther, J. H.; Jaffe, R. L.; Halicioglu, T.; Noca, F.; Koumoutsakos, P.; Ames, N.; Field, M. *Nano Lett.* **2001**, *1*, 697−702.
(40) Rafiee, J.; Mi, X.; Gullapalli, H.; Thomas, A. V.; Yavari, F.; Shi, Y.; Ajayan, P. M.; Koratkar, N. a. *Nat. Mater.* **2012**, *11*, 217−222.
(41) Yang, J.; Zhang, Z.; Men, X.; Xu, X.; Zhu, X. *Langmuir* **2010**, *26*, 10198−10202.
(42) Papadopoulos, P.; Mammen, L.; Deng, X.; Vollmer, D.; Butt, H. *Proc. Natl. Acad. Sci. U.S.A.* **2013**, *110*, 3254−3258.
(43) Zorba, V.; Stratakis, E.; Barberoglou, M.; Spanakis, E.; Tzanetakis, P.; Anastasiadis, S. H.; Fotakis, C. *Adv. Mater.* **2008**, *20*, 4049−4054.
(44) Brunet, P.; Lapierre, F.; Thomy, V.; Coffinier, Y.; Boukherroub, R. *Langmuir* **2008**, *24*, 11203−11208.
(45) McCarthy, M.; Gerasopoulos, K.; Enright, R.; Culver, J. N.; Ghodssi, R.; Wang, E. N. *Appl. Phys. Lett.* **2012**, *100*, 263701.
(46) Checco, A.; Rahman, A.; Black, C. T. *Adv. Mater.* **2013**, 1−6.
(47) Deng, T.; Varanasi, K. K.; Hsu, M.; Bhate, N.; Keimel, C.; Stein, J.; Blohm, M. *Appl. Phys. Lett.* **2009**, *94*, 133109.
(48) Brown, P. S.; Talbot, E. L.; Wood, T. J.; Bain, C. D.; Badyal, J. P. S. *Langmuir* **2012**, *28*, 13712−9.
(49) Bird, J. C.; Dhiman, R.; Kwon, H.-M.; Varanasi, K. K. *Nature* **2013**, *503*, 385−388.
(50) Park, J.-G.; Lee, S.-H.; Ryu, J.-S.; Hong, Y.-K.; Kim, T.-G.; Busnaina, A. a. *J. Electrochem. Soc.* **2006**, *153*, G811−G814.
(51) Quéré, D. *Phys. A* **2002**, *313*, 32−46.
(52) Ryan, M. E.; Fonseca, L. C.; Tasker, S.; Badyal, J. P. S. *J. Phys. Chem.* **1995**, *99*, 7060−7064.
(53) Peng, H.; Alemany, L. B.; Margrave, J. L.; Khabashesku, V. N. *J. Am. Chem. Soc.* **2003**, *125*, 15174−15182.
(54) Antonini, C.; Villa, F.; Bernagozzi, I.; Amirfazli, A.; Marengo, M. *Langmuir* **2013**, *29*, 16045−16050.
(55) Thomassin, J.-M.; Jérôme, C.; Pardoen, T.; Bailly, C.; Huynen, I.; Detrembleur, C. *Mater. Sci. Eng., R* **2013**, *74*, 211−232.
(56) Ando, Y.; Zhao, X.; Shimoyama, H.; Sakai, G.; Kaneto, K. *Int. J. Inorg. Mater.* **1999**, *1*, 77−82.
(57) Wei, T.; Song, L.; Zheng, C.; Wang, K.; Yan, J.; Shao, B.; Fan, Z.-J. *Mater. Lett.* **2010**, *64*, 2376−2379.
(58) Fan, Z.; Zheng, C.; Wei, T.; Zhang, Y.; Luo, G. *Polym. Eng. Sci.* **2009**, *49*, 2041−2045.
(59) Muthiah, P.; Bhushan, B.; Yun, K.; Kondo, H. *J. Colloid Interface Sci.* **2013**, *409*, 227−236.
(60) Tuteja, A.; Choi, W.; Ma, M.; Mabry, J. M.; Mazzella, S. a; Rutledge, G. C.; McKinley, G. H.; Cohen, R. E. *Science* **2007**, *318*, 1618−1622.
(61) Rajendra Kumar, R. T.; Mogensen, K. B.; Bøggild, P. *J. Phys. Chem. C* **2010**, *114*, 2936−2940.
(62) Mathew, T.; Datta, R. N.; Dierkes, W. K.; van Ooij, W. J.; Noordermeer, J. W. M.; Gruenberger, T. M.; Probst, N. *Carbon* **2009**, *47*, 1231−1238.
(63) Kota, A. K.; Kwon, G.; Choi, W.; Mabry, J. M.; Tuteja, A. *Nat. Commun.* **2012**, *3*, 1025.
(64) Brown, P. S.; Atkinson, O. D. L. A.; Badyal, J. P. S. *ACS Appl. Mater. Interfaces* **2014**.
(65) Zhang, W.; Shi, Z.; Zhang, F.; Liu, X.; Jin, J.; Jiang, L. *Adv. Mater.* **2013**, *25*, 2071−2076.
(66) Calcagnile, P.; Fragouli, D.; Bayer, I. S.; Anyfantis, G. C.; Martiradonna, L.; Cozzoli, P. D.; Cingolani, R.; Athanassiou, A. *ACS Nano* **2012**, *6*, 5413−5419.
(67) Wu, H.; Drzal, L. T. *Carbon* **2012**, *50*, 1135−1145.

NOTE ADDED AFTER ASAP PUBLICATION

This paper was published on the Web on May 20, 2014, with an error in the Abstract graphic. The corrected version was reposted on May 22, 2014.